Development of a Control Framework to Autonomously Install Clip Bird Diverters on High-Voltage Lines

Simone D'Angelo*, Francesca Pagano*, Fabio Ruggiero, Vincenzo Lippiello

***Abstract*— Autonomous inspection and maintenance tasks with unmanned aerial vehicles on high-voltage lines require moving in a structured environment and detecting the object to interact with. A preliminary control framework for the autonomous installation of clip bird diverters on high-voltage lines is presented in this paper. The sketched framework shows initial designs and results and underlines functionalities to be developed in the future. The idea has been validated in simulation (employing the *Gazebo* software endowed with a physics engine) through a drone equipped with a 6-degree-of-freedom robotic arm and in real experiments through a drone equipped with a sensorized stick to be compliant with the environment. This last successfully inserted the bird diverter device on a mock-up structure with minimal disturbances on the aerial platform.**

I. INTRODUCTION

In every country, thousands of kilometres of aerial power-lines represent a crucial part of the power grid system and require periodic inspection and maintenance operations. The installation of devices on the lines is one of these operations, and it has to be performed by highly trained operators because the presence of electrified conductors and the high altitude makes the workspace extremely risky for humans. In this context, the deployment of *unmanned aerial manipulators* (UAMs) promises to increase workers' safety and time efficiency and to reduce costs thanks to the ability of these platforms to reach high altitudes and operate with dexterous capabilities, exploiting a wide range of robotic configurations [1], [2].

This work is focused on a particular type of device, called *bird diverter*, that is usually installed on transmission lines. Bird diverters are marking devices, often provided with moving parts and reflectors, used to make suspended electric wires more visible to birds and thus reduce avian collisions with the lines. Although these accidents rarely cause break-outs or damage to the power infrastructure, they pose a threat to bird life, especially when power lines are placed on birds' migration routes. In fact, even if it is a largely unknown phenomenon, avian collisions with electrical infrastructures cause the death of several millions of birds [3] and represent a critical conservation issue. Different organizations world-wide published guidelines, as [4], to mitigate the impact of power lines on bird life and suggest using marking devices as a possible solution. The estimated effectiveness of bird diverters varies between studies, but they are believed to to reduce impacts up to 70% [5]. Nevertheless their actual deployment is limited due to the difficulty of installing these devices on already-built transmission lines and replacing damaged ones.

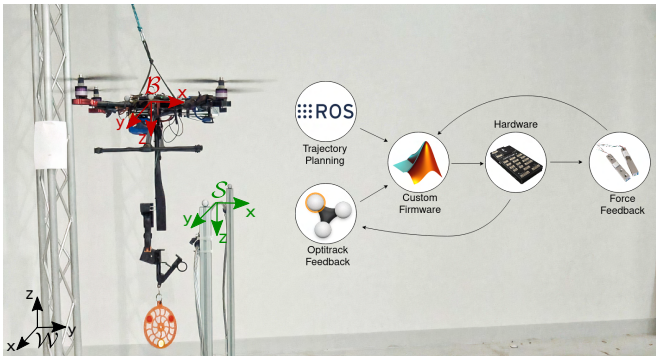

Fig. 1: Snapshot from the flight arena experiments. The drone carries the bird diverter device to install it on the cable. The main frames are depicted. Software and Hardware interconnection diagram is shown.

This work proposes the application of UAMs for the autonomous insertion of flapping, clip-type bird diverters on suspended wires to address aforementioned problems. Making the installation of bird diverters easier, safer and cheaper would encourage their use with a potentially significant impact on birdlife protection.

The paper is organized as follows: Section II introduces the current procedures for bird diverter installation and related works. The sought framework, with respect to which this papers presents a preliminary approach, is depicted in Section III. Section IV describes the control framework and the proposed technological solution. Simulations in *ROS*/*Gazebo* and real-world experimental results are reported in Sections V and VI. Finally, Section VII concludes and analyzes future work and functionalities to be developed.

II. RELATED WORKS

Bird diverters are traditionally installed manually on power-lines by workers that reach electric lines with the aid of aerial platforms, bucket trucks or helicopters. More recently, private companies have devised different solutions for easing this procedure, employing mobile robots [6], drones equipped with custom tools [7], [8], or long insulated sticks [9]. If mobile robots are semi-autonomous, drones are always remotely piloted. One of the first proofs of concept of the installation of bird diverters via a human-piloted drone can be found in [10]. However, the success

The research leading to these results has been supported by the AERIAL-CORE project (Horizon 2020 Grant Agreement No. 871479). The authors are solely responsible for its content.

* Simone D'Angelo and Francesca Pagano are both first authors.

The authors are with CREATE Consortium and PRISMA Lab, Department of Engineering and Information Technology, University of Naples Federico II, Via Claudio 21, Naples, 80125, Italy. Corresponding authors' emails: simone.dangelo@unina.it, francesca.pagano@unina.it.

of the insertion depends solely on the pilot's skills and experience as the operator has to safely handle the UAV behaviour in the hooking phase and avoid collision with lines. Moreover, many bird diverters must be installed to mark the line effectively, leading to highly repetitive labour. Developing a robust autonomous system, that also ensures the platform's stability in the hooking phase, can ease this installation process.

Within the context of the AERIAL-CORE project [11], an aerial bimanual platform is proposed to install helical bird diverters [12]; preliminary ground tests with a custom gripper are shown in [13]. Another gripper for helical bird diverter manipulation is presented in [14], but the tool was not employed on a UAV. In [15], a hardware-in-the-loop simulator of a UAM is applied to bird diverter insertion. However, the insertion experiment is conducted with a fixed manipulator and only a simulated UAM. Therein, the experiment shows interaction forces much higher than those declared by [10], probably due to different bird diverter devices employed. In [16] and [17], the prototype and experimental validation of a custom UAM system for the autonomous installation of clip-type bird diverters is presented. The aerial manipulator is a linear-actuator platform [12], i.e., a drone equipped with a manipulating tool endowed with a linear actuator that delivers the 440 N force necessary for the installation of the bird diverter chosen.

This work focuses on a different UAM instead and employs another type of clip-type bird diverter [9]. Differently, from [12], [16], [17], the presented aerial platform is made by a quadrotor endowed with a single robotic arm or a stick. This choice increases the safety distance with the line if compared to [16], [17]. It is crucial to underline that the stick configuration is similar to the commercial solution provided by [9], which is remotely piloted and sensorless.

III. GENERAL FRAMEWORK

This work aims to provide the first steps towards the development of an autonomous system able to complete the installation process of clip-like bird diverters on power-lines. The system should execute successive tasks like navigating the environment carrying multiple diverters, recognising the wire, and completing repeated installations thanks to the attached manipulator. When the UAV completes the task or a failsafe is detected, it has to return to the base and recharge the batteries and the equipment necessary to repeat the procedure. The drone should use feedback from the onboard camera system to move along the power-line and position itself. Image processing techniques will be used to find the portion of cable on which a diverter has not yet been inserted, estimate its position and create a reference trajectory that can lead the drone to complete the installation. Hooking is the most critical part of the task as it involves interaction with the power-line: an admittance controller can handle this contact phase. The impact with the cable will allow not only the coupling of the diverter but also its detachment from the drone holding clamp. A load cell connects the latter to the stick: it is a sensor composed of an electronic component

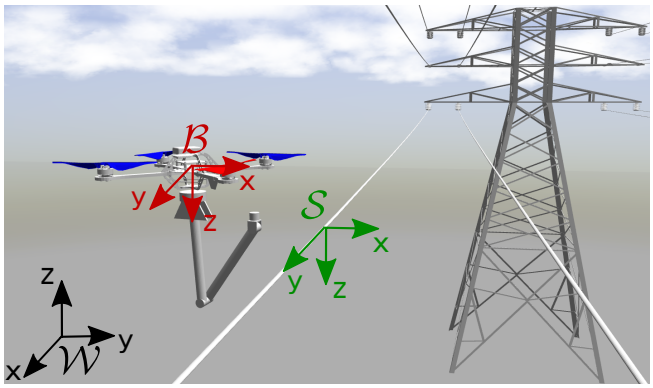

Fig. 2: Simulation scene from *Gazebo* environment with the aerial manipulator and the power-line to inspect. The main frames are depicted.

used to retrieve the force applied to an object by measuring an electrical signal which varies due to the deformation that this force produces on the bar. Its measure can also retrieve the force exerted on the cable and guarantee that the bird diverter is installed in a compliant manner without exerting a too high force that might damage the power-line.

Therefore, the control framework's objective is twofold: positioning the UAV accurately near the power-line cable and interacting with desired compliance for the task execution.

Preliminary results will be presented in this paper starting from the next Section. Basically, they are the first tests involving the navigation and bird diverter insertion phases in a controlled indoor environment where the cable position is assumed to be known. In Section VII-A, the missing steps towards the realization of the entire framework, here described, are discussed.

IV. CONTROL FRAMEWORK

A. Control Design

The devised control algorithm merges the geometric tracking controller with integral action [18] and an admittance control law [19].

With reference to Fig. 2, let $\mathcal{W}$ be the world inertial reference frame. Let $\mathcal{B}$ be the body-fixed frame whose origin is coincident with the drone's center of mass (CoM) and $\mathcal{S}$ be the frame attached to the power-line cable. The linear position and velocity of $\mathcal{B}$ in $\mathcal{W}$ are denoted by $p, v \in \mathbb{R}^3$. The matrix $R \in SO(3)$ is the orientation defined as the linear transformation of a vector from $\mathcal{B}$ to $\mathcal{W}$, while $\omega \in \mathbb{R}^3$ is the angular velocity vector defined in $\mathcal{B}$. The set of equations describing the UAV motion are given by

$$\begin{aligned} \dot{p} &= v, \\ m\dot{v} &= mge_3 - u_T R e_3, \\ \dot{R} &= R\hat{\omega}, \\ J\dot{\omega} + \omega \times J\omega &= \tau_{des}, \end{aligned} \tag{1}$$

where $m \in \mathbb{R}$ and $J \in \mathbb{R}^{3\times3}$ denote the mass and the inertial matrix of the UAV, respectively; $g = 9.81\ m/s^2$ is the gravity acceleration, and $e_3 = \begin{bmatrix} 0 & 0 & 1 \end{bmatrix}^T$ is a unit vector defining the direction of the total thrust. The sum of each propeller thrust returns the value of the total thrust $u_T = \sum_{i=1}^{4} f_i \in \mathbb{R}$, whose direction is normal to the multi-rotor plane; its

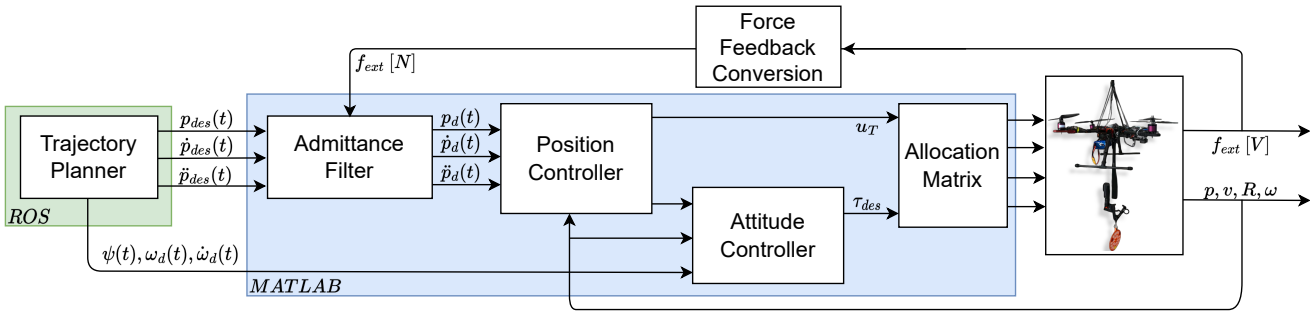

Fig. 3: Overall control scheme. The offline trajectory planner returns the inputs to an admittance control scheme in the Cartesian space. At each sample time, the control inputs are computed to track the desired references. When the end-effector goes in contact with the cable, the admittance filter computes the correction on the reference trajectory from the interaction force measures.

magnitude and the total moment, $\tau_{des} \in \mathbb{R}^3$ expressed in the body-fixed frame, are the control inputs of system in (1). Finally, the hat operator, as in $\hat{\omega}$, transforms a vector from $\mathbb{R}^3$ into the corresponding skew-symmetric matrix belonging to $so(3)$.

The control inputs are related to the thrusts of the UAV rotors, $f_i \in \mathbb{R}$, with $i = 1, \dots, 4$, through an allocation matrix as follows

$$\begin{bmatrix} \tau_1 \\ \tau_2 \\ \tau_3 \\ u_T \end{bmatrix} = \underbrace{\begin{bmatrix} \sin(\theta_1)d & d\sin(\theta_2) & d\sin(\theta_3) & d\sin(\theta_4) \\ d\cos(\theta_1) & d\cos(\theta_2) & d\cos(\theta_3) & d\cos(\theta_4) \\ k_m & k_m & -k_m & -k_m \\ -1 & -1 & -1 & -1 \end{bmatrix}}_{A} \begin{bmatrix} f_1 \\ f_2 \\ f_3 \\ f_4 \end{bmatrix}, \quad (2)$$

where $d > 0$ is the distance between each propeller and the UAV's CoM, $\theta_i \in \mathbb{R}$ is the fixed angular position of i-th propeller with respect to $\mathcal{B}$, while $k_m, k_f \in \mathbb{R}$ are two aerodynamic parameters, with $f_i = k_f w_i^2$, being $\omega_i \in \mathbb{R}$ the velocity of the i-th UAV propeller.

Given a reference trajectory in terms of $p_d(t), \dot{p}_d(t), \ddot{p}_d(t) \in \mathbb{R}^3$, the tracking errors for the linear position and velocity are

$$e_p(t) = p(t) - p_d(t), \quad (3)$$
$$e_v(t) = v(t) - \dot{p}_d(t), \quad (4)$$
$$e_i(t) = \int_0^t \big(e_v(\tau) + c_1 e_x(\tau)\big) d\tau, \quad (5)$$

the last term is an integral action as introduced in [18], where the constant $c_1 \in \mathbb{R}$ is used to prove the exponential stability of the tracking error at steady state. All the considerations therein are the same. From these quantities the total thrust is computed as

$$u_T = (K_P e_p(t) + K_D e_v(t) + K_I sat_\sigma(e_i(t)) + mge_3 - m\ddot{p}_d(t)) \cdot Re_3, \quad (6)$$

where $K_P, K_D, K_I \in \mathbb{R}^{3\times3}$ are respectively the proportional, derivative, and integral gains and the operator $\cdot$ represents the scalar product. A saturation is added on the integral action as

$$sat_\sigma(e_i(t)) = \begin{cases} \sigma & e_i(t) > \sigma \\ e_i(t) & -\sigma \le e_i(t) \le \sigma, \\ -\sigma & e_i(t) < -\sigma \end{cases} \quad (7)$$

keeping constant the value of $e_i(t)$ outside the range defined by the constant $\sigma \in \mathbb{R}^+$: $sat_\sigma(e_i(t)) : \mathbb{R} \to [-\sigma, \sigma]$.

In a similar way, given the desired attitude matrix $R_d \in SO(3)$, computed from the yaw reference $\psi_d(t) \in \mathbb{R}$, and the desired body angular velocity $\omega_d \in \mathbb{R}^3$, the angular position errors are defined as

$$e_R(t) = \frac{1}{2}(R_d^T R - R^T R_d)^\vee, \quad (8)$$
$$e_\omega(t) = \omega - R^T R_d \omega_d, \quad (9)$$

where the $\vee$ operator is the inverse of the hat operator. Again, an integral action is introduced also for the attitude control as

$$e_i(t) = \int_0^t \big(e_\omega(\tau) + c_2 e_R(\tau)\big) d\tau. \quad (10)$$

The constant $c_2 \in \mathbb{R}^+$ has the same role of c_1 in (5). From these quantities, considering the matrix $K_R, K_\omega, K_{I_o} \in \mathbb{R}^{3\times3}$ as proportional derivative and integral gains, the desired moments are computed as follows

$$\tau_{des} = -K_R e_R - K_\omega e_\omega - K_{I_o} e_i + \omega \times J\omega - J(\hat{\omega} R^T R_d \omega_d - R^T R_d \dot{\omega}_d). \quad (11)$$

Equations (6) and (11) are then converted into the propellers' angular velocities through (2).

The admittance control law derives from the impedance controller [19]. As shown in Fig. 3, the filter interposes between the planner and the controller, defining a compliant frame on the basis of the measure of the force sensor. The force feedback is used to correct the motion references only in the direction of the interaction to obtain the desired active compliance with the environment. The filter takes as input the planner output, $p_{des}(t), \dot{p}_{des}(t), \ddot{p}_{des}(t) \in \mathbb{R}^3$, and it is defined as

$$M_a \ddot{z}(t) + K_{p_a} z(t) + K_{d_a} \dot{z}(t) = f_{ext}(t), \quad (12)$$

where $z(t) \in \mathbb{R}^3$ is the error between the trajectory planner output and the reference given to the UAV position controller, $p_d(t), \dot{p}_d(t), \ddot{p}_d(t)$, taking into account the force measure for compliance purposes; $M_a, K_{d_a}, K_{p_a} \in \mathbb{R}^{3\times3}$ represent the mass, damping, and stiffness matrices, respectively, of the devised filter. Starting from the interaction force measures $f_{ext} \in \mathbb{R}^3$, the filter modifies the drone's planned references

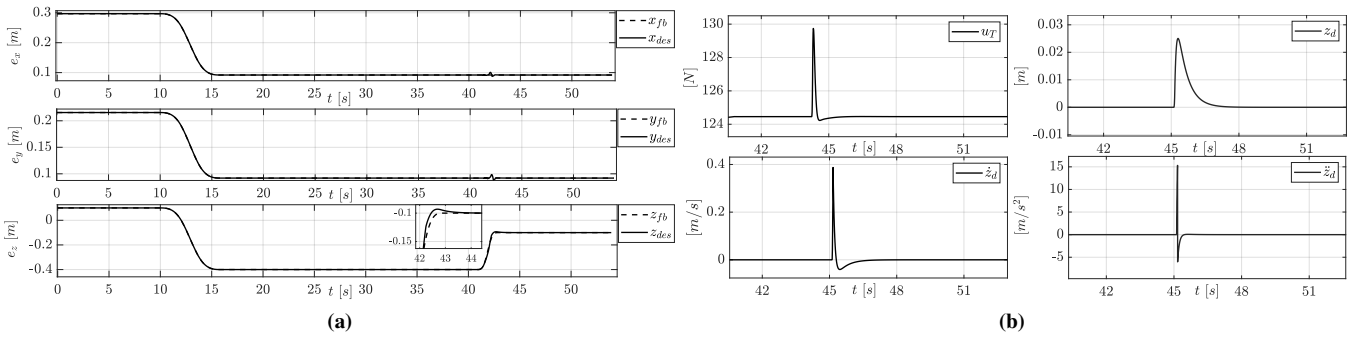

Fig. 4: Simulated experiment in *Gazebo* physic engine: (a)-End-Effector Linear Position error along the three Cartesian axis. A zoom on the position error in z is shown: it corresponds to the detachment phase of the diverter. (b)-Only the installation phase is showed. In order from the top: Total thrust given by the propeller; z_d,$\dot{z}_d$,$\ddot{z}_d$ operational space position, velocity and acceleration errors between the desired frame and the compliant one.

computing the corresponding corrections $z(t)$, $\dot{z}(t)$, $\ddot{z}(t) \in \mathbb{R}^3$. From (12), inverting the filter expression, it is possible to retrieve the acceleration

$$\ddot{z}(t) = \frac{f_{ext}(t) - K_{p_a} z(t) - K_{d_a} \dot{z}(t)}{M_a}, \tag{13}$$

while $\dot{z}(t)$ and $z(t)$ can be computed as successive time integration. Notice that, in the absence of contacts, the algorithm is a pure motion tracking controller.

B. System implementation

The controller has been developed entirely in *MATLAB* using the *UAV Toolbox Support Package for PX4 Autopilots* [20] that allows to modify and overwrite the standard *PX4* flight controller firmware. The tool offers full compatibility with different versions of the Pixhawk [21] family and the ground control station *QGroundControl* [22]. The standard *PX4 Autopilot* can already control a UAV in the Cartesian space, but problems arise when the drone has to interact with the environment. It is desirable to add some capabilities and other sensors to handle the interaction, preserving stable hovering and trajectory tracking. The *PX4* firmware structure is challenging to master and even more to modify, introducing custom controllers. Great integration with the powerful features offered by *MATLAB* and *SIMULINK* has allowed to overcome these limitations and create ad-hoc modules and messages. Overwriting the flight controller it is possible to convert the desired thrust and torques in *PWM* signals and control the motors directly, bypassing the classical *PX4* mixing system.

The overall control scheme implemented so far is presented in Fig. 3 and discussed in the previous subsection. The user must define the desired set points and the time to reach the destination. The offline planner computes the path and the trajectory using an interpolation based on splines. The results are discretized and sent to the flight controller through custom *MAVROS* messages, and the system behaves like an offboard flight mode. The hooking phase trajectory is planned so that interaction with the cable occurs when the velocity is maximum. A force sensor measures the contact force with the cable sending the data through serial communication to the developed firmware. The onboard computer executes the trajectory planner module in a ROS node. Whereas at the same time, the admittance filter, position and attitude controllers, and the allocation are embedded in the custom developed *PX4* firmware and executed on the flight controller.

V. SIMULATIONS

A. Simulation setup

Simulations have been carried out in *ROS Melodic* and *Gazebo v9.0* with simulator in [15]. The simulated UAM has a quadrotor as UAV and it is endowed with a six-DoF robotic arm. The control architecture is decoupled: the geometric flight controller [18] for the aerial platform and an admittance controller based on the inverse dynamic control law for the six-DoF manipulator. The decoupling is ensured in quasi-stationary flight conditions. An external wrench estimator based on momentum [23] estimates external forces and coupling effects exerted during the interaction and due to the presence of the arm. A plugin in *Gazebo* simulates the interaction forces exchanged with the line during the bird diverter installation. The plugin simulates the presence of the cable, modelling it with an elastic constant $k = 1.4\ kN/m$, chosen on the basis of experimental measurements. The force is applied only along the z-axis of $\mathcal{W}$ and released when it reaches 20 N, simulating the diverter hooking and its detachment from the holding clamp. The simulated UAM is composed by the AscTec Hummingbird quadrotor from RotorS simulator [24] and an antropomorphic arm with spherical wrist. The arm has mass $m_a = 0.97$ kg and maximum length $l_a = 0.17$ m, while the aerial platform has mass $m = 11.68$ kg and inertia matrix $J = \begin{bmatrix}0.777 & 0.777 & 1.112\end{bmatrix} I_3$ kgm^2. The tracking and admittance controller gains are $K_P = \begin{bmatrix}20 & 20 & 50\end{bmatrix} I_3$, $K_D = \begin{bmatrix}16 & 3 & 16\end{bmatrix} I_3$, $K_R = \begin{bmatrix}120 & 120 & 60\end{bmatrix} I_3$, $K_\omega = \begin{bmatrix}30 & 30 & 20\end{bmatrix} I_3$, $M_a = 3$, $K_{p_a} = 75$, $K_{d_a} = 27$.

B. Simulation results

Simulation results showed that the decoupled architecture is effective, in practice, for this installation task despite the presence of sustained and near impulsive forces. The end-effector cartesian space trajectory has been planned to reduce disturbances on the aerial platform and not mining stability.

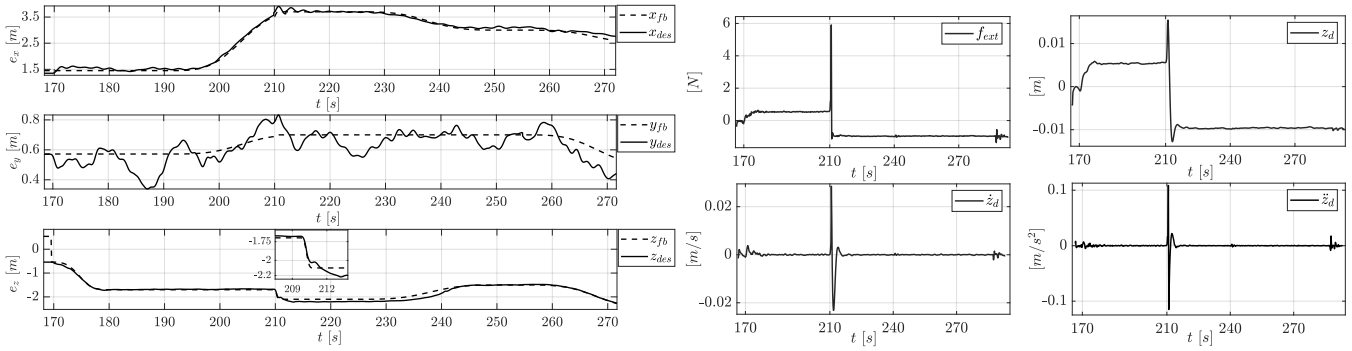

(a) **(b)**

Fig. 5: Real experiment in flight arena: (a)-Reference and actual position along the three Cartesian axis. The feedback is obtained from *OptiTrack* motion capture system. The drone is able to track the desired trajectory. Oscillations can be noticed on the y-axis. Opening the landing gears, the inertia around this axis changes, the controller can keep the drone stable despite these uncertainties. A zoom on the position error in the z component is shown: it corresponds to the detachment phase of the diverter. (b)-From the top: force feedback measured during the task execution: the initial displacement is caused by the diverter weight itself; z_d,$\dot{z}_d$,$\ddot{z}_d$ are the filters outputs used to correct the trajectory references.

The desired trajectory drives the device in contact with the cable when the end-effector velocity is maximum, commanding a displacement of 30 cm along the vertical axis in 2 s. Plots of the hooking phase are depicted: in ideal conditions and without external disturbances in Fig. 4-(a) the aerial manipulator perfectly tracks the desired trajectory during the installation process. The total thrust and the relative trajectory corrections are presented in Fig. 4-(b). The thrust change is due to the estimated external force exerted on the aerial platform during the device installation, while torques have not been depicted because they minimally affect the hovering condition.

VI. REAL WORLD EXPERIMENTS

A. Experimental setup

Real experiments were performed in a controlled environment, an indoor flight arena, with an ad-hoc setup mimicking a high-voltage line with a real power-line conductor and an *OptiTrack-Motion Capture System* [25] to retrieve the drone position and velocity feedback.

Simulations in Section V motivated the mechatronic design of the first simplified prototype as visible in Fig. 1. The arm is replaced by a stick with a sensor that measures only the force along the drone z-axis of $\mathcal{B}$, while the vertical configuration minimizes external torques on the aerial platform.

The employed drone is a quadrotor UAV made with Tarot 650 sport commercial frame, Hacker A30-14L (800 rpm/V) brushless motors and 14×4.7 inch propellers. The frame has been customized with a 40 cm stick composed of carbon fibre tube, 3D printed elements, a force sensor, and a clip on its tip. Finally, an actuated landing gear, directly controlled by *PWM* signals, allows sufficient free space for the device installation, given the chosen configuration. The system's total weight is 3.7 kg.

The force sensor connected to the end-effector clip is a load cell with a maximum nominal load of 5 kg. The force feedback is handled by an Arduino Nano board which converts the analogic measure to two strings of 1 byte. The board sends them to the *Pixhawk* flight controller through serial communication. Then, the measure is reconstructed and converted into a force message to be used in the admittance control law and published as an uORB topic. All the computations are performed by an onboard Intel UP computer connected to a *Pixhawk 4* flight controller.

The motion controller dynamical parameters are selected from the CAD model of the drone and they are $m = 3.7$ kg, $J = \begin{bmatrix}0.0252 & 0.0458 & 0.057\end{bmatrix} I_3$ kgm^2, whereas the allocation matrix parameters are chosen equal to $d = 0.30$ m, $\theta_1 = \frac{\pi}{4}$, $\theta_2 = \frac{5\pi}{4}$, $\theta_3 = -\frac{\pi}{4}$, $\theta_4 = -\frac{5\pi}{4}$, $k_f = 2.20$ and $k_m = 0.1759$. The sampling time is set to $T_s = 0.004$ s and the controller gains are $K_P = \begin{bmatrix}10 & 10 & 60\end{bmatrix} I_3$, $K_D = \begin{bmatrix}5.3 & 5.3 & 32\end{bmatrix} I_3$, $K_I = \begin{bmatrix}3 & 3 & 3\end{bmatrix} I_3$, $K_R = \begin{bmatrix}6 & 7 & 8\end{bmatrix} I_3$, $K_\omega = \begin{bmatrix}1 & 2 & 3.5\end{bmatrix} I_3$, $K_{I_o} = \begin{bmatrix}0.2 & 0.3 & 0.3\end{bmatrix} I_3$, $M_a = 30$, $K_{p_a} = 100$, $K_{d_a} = 100$. The prototype has different dynamic characteristics compared to the simulated platform, requiring additional tuning steps for the controller gains. Furthermore, the admittance filter gains are chosen to avoid acceleration corrections with high values.

B. Experimental validation

To analyze the behaviour of the system during the task execution, both the contact-less flight phase and the contact one were tested, showing stable flight with the implemented controller. The experiments impose a constant yaw-angle reference during the whole task execution.

As shown in Fig. 5-(a), the UAV can track the desired trajectories with small errors. When the landing gear is activated, the inertia along the y-axis changes. However, we opted for a static inertia matrix not accounting for this variation. Landing legs are made of lightweight carbon fibre and it is possible to observe decreasing oscillations and a stabilizing effect in the positioning near the line.

The interaction occurs around 210 s as shown in Fig. 5: the load cell measures the contact force along the z-axis with a maximum value of 6 N, used by the admittance controller. The drone remains stable also after releasing the clip on the desired cable section. The plots in Fig. 5-(b) show

the admittance filter input and outputs computed during the interaction. The difference in the force measured along the z-axis by the load cell in Fig. 5-(b) is due to the weight of the bird diverter that has been released. It is worth underlining that in the performed experiments the measured 6 N force is not necessary for the closure of the clip but for the detachment of the diverter from the holding claw. Notice that the measured force is lower than the one simulated, which was chosen in conservative manner.

Experiments showed that the drone can go in contact with the cable, withstand the forces exchanged during the interaction, and correctly install the bird diverter on the wire. Albeit the positioning along the drone y-axis is not accurate, the installation can be executed with an acceptable error since bird diverters are usually installed on the lines every 10 m. Better performances can be obtained accounting for the varying inertia matrix and with a better tuning of the gains.

VII. CONCLUSIONS

This work tackles the problem of performing bird diverters installation with an aerial manipulator. Preliminary tests demonstrate that the prototype can complete the assigned task, taking advantage of an admittance control law which gives to the system the desired compliance with the environment. The whole controller is implemented inside the *PX4* flight controller using the *MATLAB* toolbox: it was possible to use the powerful features of *MATLAB* and *SIMULINK* environments to program and test the controller with great integration with the standard *PX4 Autopilot*. This framework tracks the desired position and uses the force measured at the robot's tip to complete the installation without losing stability.

A. Future and on-going developments

The obtained preliminary results are fundamental to continue the framework development. Future work involves testing different techniques to detect the power-line cable in the environment. Onboard camera sensors will be used to integrate this task thanks to image elaboration techniques like classic visual servoing algorithms or more promising deep learning-based libraries, such as YOLO. The final step will be to fuse the visual and force feedback in a hybrid control law in the image space.

The presented prototype can also be modified to carry multiple diverters simultaneously for successive installations. The future versions of this hardware will be closer to the simulated UAM in Fig.2 considered during preliminary tests. A manipulator enlarges the workspace: considering an over-actuated system, it will be possible to complete some sub-tasks like picking another diverter from the onboard drone equipment and repeating the installation process without returning to the base station. Finally, tests in a real outdoor scenario will be performed.

REFERENCES

[1] F. Ruggiero, V. Lippiello, and A. Ollero, "Aerial manipulation: A literature review," *IEEE Robotics and Automation Letters*, vol. 3, no. 3, pp. 1957–1964, 2018.

[2] A. Ollero, M. Tognon, A. Suarez, D. Lee, and A. Franchi, "Past, present, and future of aerial robotic manipulators," *IEEE Transactions on Robotics*, vol. 38, no. 1, pp. 626–645, 2022.

[3] S. Loss, T. Will, and P. Marra, "Refining estimates of bird collision and electrocution mortality at power lines in the united states," *PloS one*, vol. 9, p. e101565, 07 2014.

[4] A. P. L. I. Committee, *"Reducing avian collisions with power lines, the state of the art in 2012."*. Edison Electric Institute EEI, 2012.

[5] M. Ferrer, V. Morandini, R. Baumbusch, R. Muriel, M. De Lucas, and C. Calabuig, "Efficacy of different types of "bird flight diverter" in reducing bird mortality due to collision with transmission power lines," *Global Ecology and Conservation*, vol. 23, p. e01130, 2020. [Online]. Available: https://www.sciencedirect.com/science/article/pii/S2351989420306715

[6] "Fulcrumair," https://fulcrumair.com/bird-flight-diverters/, accessed: 2022-12-29.

[7] "Plp. drone installation." https://www.youtube.com/watch?v=PfkRt2W7NAk, accessed: 2022-12-29.

[8] "P&r tech. bird diverter," https://pr-tech.com/product/birdmark-bird-diverter/, accessed: 2022-12-29.

[9] "Crocfast. drone installation," https://birddiverter.eu/drone-installation, accessed: 2022-12-29.

[10] S. Lobermeier, M. Moldenhauer, C. M. Peter, L. Slominski, R. A. Tedesco, M. Ver Meer, J. F. Dwyer, R. E. Harness, and A. H. Stewart, "Mitigating avian collision with power lines: a proof of concept for installation of line markers via unmanned aerial vehicle," *Journal of Unmanned Vehicle Systems*, vol. 3, no. 4, pp. 252–258, 2015. [Online]. Available: https://doi.org/10.1139/juvs-2015-0009

[11] "Aerial-core project home page," https://aerial-core.eu/, accessed: 2022-12-29.

[12] J. Cacace, S. M. Orozco-Soto, A. Suarez, A. Caballero, M. Orsag, S. Bogdan, G. Vasiljevic, E. Ebeid, J. A. A. Rodriguez, and A. Ollero, "Safe local aerial manipulation for the installation of devices on power lines: Aerial-core first year results and designs," *Applied Sciences*, vol. 11, no. 13, 2021. [Online]. Available: https://www.mdpi.com/2076-3417/11/13/6220

[13] I. Armengol, A. Suarez, G. Heredia, and A. Ollero, "Design, integration and testing of compliant gripper for the installation of helical bird diverters on power lines," 10 2021, pp. 1–8.

[14] J. Cacace, L. Giampetraglia, F. Ruggiero, and V. Lippiello, "A novel gripper prototype for helical bird diverter manipulation," *Drones*, vol. 7, no. 1, 2023. [Online]. Available: https://www.mdpi.com/2504-446X/7/1/60

[15] E. Cuniato, J. Cacace, M. Selvaggio, F. Ruggiero, and V. Lippiello, "A hardware-in-the-loop simulator for physical human-aerial manipulator cooperation," in *2021 20th International Conference on Advanced Robotics (ICAR)*, 2021, pp. 830–835.

[16] A. Rodriguez-Castaño, S. R. Nekoo, H. Romero, R. Salmoral, J. A. Acosta, and A. Ollero, "Installation of clip-type bird flight diverters on high-voltage power lines with aerial manipulation robot: Prototype and testbed experimentation," *Applied Sciences*, vol. 11, no. 16, 2021. [Online]. Available: https://www.mdpi.com/2076-3417/11/16/7427

[17] A. Suarez, H. Romero, R. Salmoral, J. A. Acosta, J. Zambrano, and A. Ollero, "Experimental evaluation of aerial manipulation robot for the installation of clip type bird diverters: Outdoor flight tests," in *2021 Aerial Robotic Systems Physically Interacting with the Environment (AIRPHARO)*, 2021, pp. 1–7.

[18] F. Goodarzi, D. Lee, and T. Lee, "Geometric nonlinear pid control of a quadrotor uav on se(3)," pp. 3845–3850, 2013.

[19] B. Siciliano, L. Sciavicco, L. Villani, and G. Oriolo, *"Robotics: Modelling, Planning and Control"*. Springer, 2009.

[20] MATLAB PX4 Toolbox, https://it.mathworks.com/help/supportpkg/px4/index.html.

[21] "Px4 home page," https://pixhawk.org/, accessed: 2023-01-4.

[22] "Qgc home page," http://qgroundcontrol.com/, accessed: 2023-01-4.

[23] F. Ruggiero, J. Cacace, H. Sadeghian, and V. Lippiello, "Passivity-based control of vtol uavs with a momentum-based estimator of external wrench and unmodeled dynamics," *Robotics Auton. Syst.*, vol. 72, pp. 139–151, 2015.

[24] F. Furrer, M. Burri, M. Achtelik, and R. Siegwart, *Robot Operating System (ROS): The Complete Reference (Volume 1)*. Cham: Springer International Publishing, 2016, ch. RotorS—A Modular Gazebo MAV Simulator Framework, pp. 595–625. [Online]. Available: http://dx.doi.org/10.1007/978-3-319-26054-9_23

[25] "Optitrack home page," https://optitrack.com/, accessed: 2023-01-4.